PHYSICAL REVIEW B, VOLUME 63, 060502(R)

Anomalies in the infrared spectra of underdoped $Bi_2Sr_2CaCu_2O_z$ as evidence for the intrabilayer Josephson effect

V. Železný,[1,*] S. Tajima,[1] D. Munzar,[2] T. Motohashi,[3] J. Shimoyama,[3] and K. Kishio[3]
[1]*Superconductivity Research Laboratory-ISTEC, Tokyo 135-0082, Japan*
[2]*Department of Solid State Physics, Masaryk University, Kotlářská 2, CZ-61137 Brno, Czech Republic*
[3]*Department of Applied Chemistry, The University of Tokyo, Tokyo 113-8656, Japan*
(Received 22 September 2000; published 16 January 2001)

It was found that the *c*-axis optical conductivity spectra of underdoped $Bi_2Sr_2CaCu_2O_z$ exhibit an anomalous increase of the electronic background around 450 cm^{-1} below T_c, accompanied by several phonon anomalies. Our observations confirm that these features, so far observed only in high-T_c compounds with considerably higher *c*-axis conductivity, are common in the family of underdoped bilayer cuprates. The data can be well understood within a model involving variations of the electric field inside the unit cell and the intrabilayer Josephson effect. Some differences from the cases of the other cuprates are attributed to a highly insulating property of the blocking layers.

DOI: 10.1103/PhysRevB.63.060502 PACS number(s): 74.72.Bk, 74.25.Gz, 74.25.Kc, 74.50.+r

The *c*-axis infrared conductivity of the high-T_c superconductors (HTSC) is one of the most unconventional properties of these materials. The spectra of the underdoped compounds[1,2] are characterized by low electronic background and well-developed phonon peaks. A dramatic change from an incoherent charge dynamics in the normal state into a coherent one below T_c is the appearance of a sharp reflectivity edge, the so-called Josephson plasma[3] below T_c. Another remarkable feature is a growth of the bump around 450 cm^{-1} at low temperatures in underdoped $YBa_2Cu_3O_{7-\delta}$ (Y123), accompanied by several phonon anomalies. This phenomenon has been found not only in underdoped Y123,[1] but also in $YBa_2Cu_4O_8$ (Ref. 4) and $Pb_2Sr_2(Y/Ca)Cu_3O_8$,[5] all of which show relatively high conductivity in the *c*-direction.

The origin of the bump and phonon anomalies has been a mystery for a long time, while some research groups discussed it in relation with a spin gap.[6] Recently, van der Marel and Tsvetkov[7] proposed an idea that the spectral growth around 450 cm^{-1} results from the intrabilayer Josephson effect. This idea can be valid if the same phenomenon occurs in all the HTSC with a double CuO-pyramid, irrespective of the *c*-axis conductivity.

In this paper, we report on our studies of the infrared *c*-axis response of another typical double layer material, but with low conductivity and high anisotropy-underdoped $Bi_2Sr_2CaCu_2O_z$ (Bi2212). We observed an anomalous behavior around 450 cm^{-1} at low temperature, which suggests a new excitation related to Josephson tunneling between two closely spaced CuO_2 planes. We can fit and understand the main features in the spectra using a model similar to that for Y123. We also demonstrate the crucial role of local field effects for understanding the anomalies.

Our measurements were carried out on two mosaics with $T_c=80$ K and $T_c=60$ K, each consisting of about 25 single crystals. The crystals were grown from feed rods by the floating-zone technique using an image furnace equipped with a double ellipsoidal mirror. Further details on the crystal growth were described elsewhere.[8] The as-grown crystals were annealed in a sealed quartz tube with an appropriate oxygen pressure for the 80 K sample and in a vacuum furnace (1.1×10^{-5} Torr) at 600 °C for the 60 K sample to reduce their oxygen content. The values of T_c were determined by magnetic measurement. The mosaics of effective surface area of $ac=3\times1.5$ mm^2 were prepared by burying the crystals in epoxy and polishing them together with epoxy to optical glance. The reflectance spectra were measured between 50 and 4000 cm^{-1}. We also proved that the reflectance of the epoxy plate is frequency independent and approximately equal to 6%. Therefore, it introduces no extra features in the mosaic spectra. We estimated a fraction of the actual surface area of the crystals and we calibrated our reflectance spectra by this fraction. The room temperature spectra of the present samples are in reasonable agreement with that of an optimally doped single crystal.[9]

Figure 1 shows the *c*-polarized reflectance spectra of Bi2212 with $T_c=80$ K in the far-infrared region for selected temperatures between 7 to 300 K. The optical conductivity, $\sigma(\omega)=\sigma_1(\omega)+i\sigma_2(\omega)$, determined by the Kramers-Kronig analysis of the reflectance, is plotted in Figs. 2(a) and 2(e) for the mosaic with $T_c=80$ K and $T_c=60$ K, respectively. The spectra of both mosaics have semiconductive character; i.e., a relatively low reflectance, the contribution of the elec-

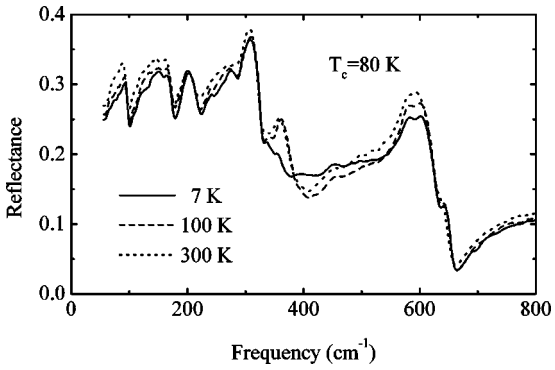

FIG. 1. Temperature dependence of the *c*-axis reflectance for the $T_c=80$ K sample.

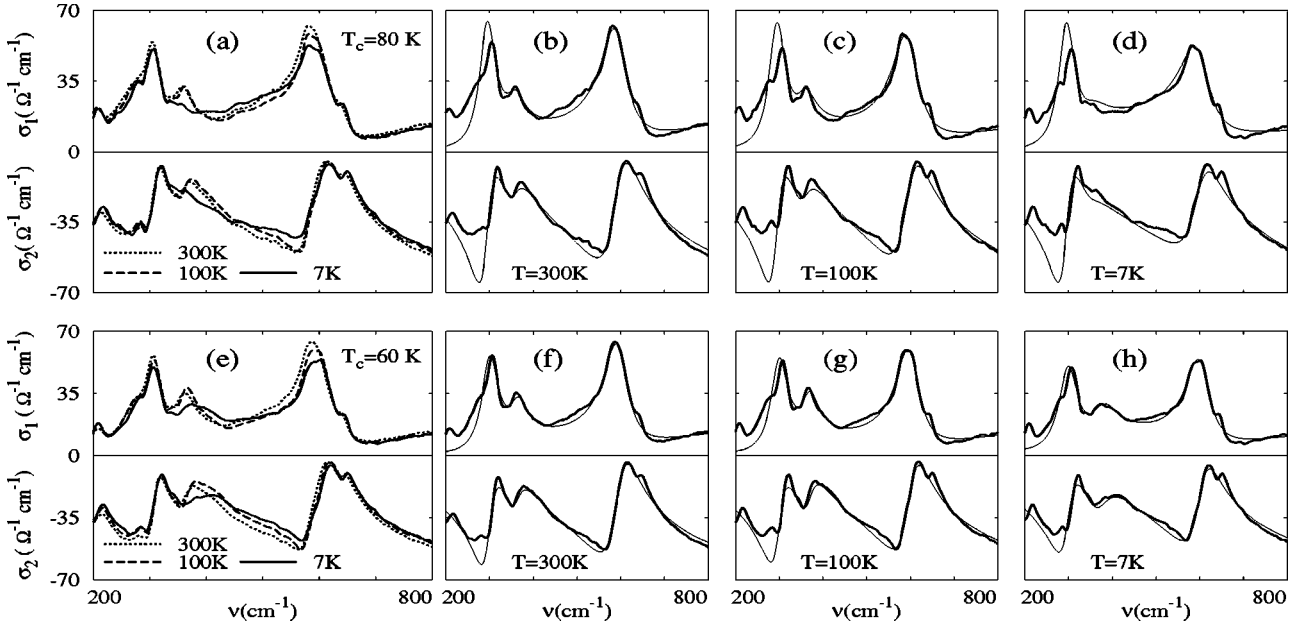

FIG. 2. (a) Experimental spectra of the real and imaginary parts of the *c*-axis conductivity for the $T_c=80$ K sample. Experimental data (thick lines) and fits (thin lines) for $T=300$ K (b), $T=100$ K (c), and $T=7$ K (d). The same plots for the $T_c=60$ K sample are shown in panels (e), (f), (g), and (h). The fitting parameters are given in Ref. 18.

tronic background to $\sigma(\omega)$ is small and most of the spectral weight is due to the six infrared active phonons at 95, 169, 208, 305, 366, and 585 cm^{-1} predicted by group analysis. As temperature decreases, several additional features appear. The phonon peak at 366 cm^{-1} first sharpens and then loses its intensity. At the same time, both the reflectance and $\sigma_1(\omega)$ minima at 450 cm^{-1} start to rise and the valley fills in. Figure 3 shows the difference $\sigma_1(7\ \mathrm{K})-\sigma_1(100\ \mathrm{K})$, illustrating the enhancement of the electronic background between 400 and 550 cm^{-1} and the strong suppression of the phonon peak at 366 cm^{-1}. It can also be seen that the spectral enhancement is slightly shifted towards lower frequencies with reducing the doping level, which can be understood as the result of decrease of the Josephson plasma frequency.

In Fig. 2, besides $\sigma_1(\omega)$ and $\sigma_2(\omega)$, their fits are also displayed. Before discussing them, we outline the main ideas

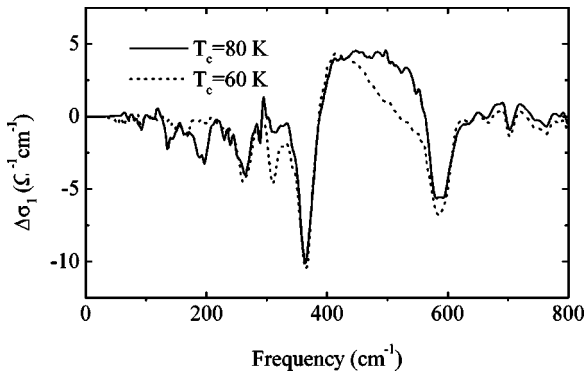

FIG. 3. Frequency dependence of the conductivity difference $\Delta\sigma=\sigma_1(7\ \mathrm{K})-\sigma_1(100\ \mathrm{K})$ for the $T_c=80$ K and $T_c=60$ K samples.

of the model. The extremely short coherence length along the *c*-axis justifies the use of the Lawrence and Doniach model,[10] i.e., treating HTSC as a stacked array of two-dimensional superconducting CuO_2 layers. The layers are separated by insulating layers and coupled by Josephson mechanism. This picture has been verified by the observations of the dc and ac intrinsic Josephson effects[11] and the Josephson plasma resonances in the microwave region.[12] Recently, van der Marel and Tsvetkov[7,13] (MT) generalized the model to the superconductors containing two CuO_2 layers per unit cell. The dielectric function of the model has two zero-crossing points, which correspond to the two Josephson plasmons: interbilayer and intrabilayer. In addition, it exhibits a pole between the two points, resulting in a new transverse excitation.[14] They suggested to attribute the bump at 450 cm^{-1} in Y123 to this excitation. On the other hand, Shibata and Yamada observed two absorption features in the T^* phase of $SmLa_{1-x}Sr_xCuO_{4-\delta}$ (Ref. 15) that confirm the existence of the two plasmons.

Taking into account local field effects explicitly, Munzar *et al.*[16] further extended the model and successfully explained most of the spectral changes including the phonon anomalies. The essential physical ideas beyond the (MT) picture are as follows. The applied electric field induces currents in the superconductor. Owing to the spatial variations of the local currents, the CuO_2 planes get charged and the resulting dipole moment is responsible for the new absorption band in the spectrum. The observed renormalizations of the phonons, in particular the change of the oxygen bond-bending mode, can be explained by the interaction between the charge carriers and the phonons mediated by the local fields.

The main features of the *c*-axis conductivity of Bi2212 are similar to those of underdoped Y123, therefore, we adapt

the model used in Ref. 16, keeping the same notation. To describe the optical response of Bi2212 with small contribution of charge carriers, we modify the charge carrier susceptibilities in the fitting approach as follows: (i) The inter-bilayer region is assumed to be insulating, i.e., the inter-bilayer susceptibility ($\chi_{\rm int}$) is set equal to zero. (ii) The intra-bilayer conductivity $\sigma_{\rm bl}$ of the following form is used:

$$\sigma_{\rm bl}(\omega) = -i\omega\epsilon_0(\epsilon_\infty + \chi_{\rm bl}(\omega))$$

and

$$\chi_{\rm bl}(\omega) = -\frac{\omega_{\rm bl}^2}{\omega^2} - \frac{\Omega_{\rm bl}^2}{\omega(\omega + i\gamma_{\rm bl})} + \frac{S_b\omega_b^2}{\omega_b^2 - \omega^2 - i\omega\gamma_b}, \quad (1)$$

where $\omega_{\rm bl}$ is the frequency of the intrabilayer Josephson plasmon. The second and third terms represent the electronic background. Here $\Omega_{\rm bl}$ and $\gamma_{\rm bl}$ are the plasma frequency and damping for the Drude term; S_b, ω_b, and γ_b are the oscillator strength, resonant frequency, and damping for the Lorenzian term. For simplicity, we include only the three phonons at 300, 366, and 585 cm^{-1} in the fitting procedure. The structural similarity to Y123 leads us to assume that the strongly renormalized phonon at 366 cm^{-1} involves mainly vibrations of the planar oxygen and the phonons at 300 and 585 cm^{-1} correspond to vibrations of the inter-bilayer ions such as apical and BiO layer oxygen. This assignment is also in qualitative agreement with the early lattice dynamical calculations.[17] The fitting was done in the spectral range from 300 to 1000 cm^{-1} and the results are shown in Fig. 2 and Ref. 18. The phonon parameters are denoted by $(\omega_P, \gamma_P, S_P)$ for the 366 cm^{-1} mode and $(\omega_i, \gamma_i, S_i;\ i=1$ and 2) for the other two. The low conductivity along the *c*-axis in Bi2212 is due to the blocking inter-bilayers. They are formed by Bi and Sr oxides that interact very weakly in the *c*-direction, as is demonstrated by the easy cleavage of Bi2212 crystal perpendicularly to this direction. This results in the positive and large real part of the dielectric function ($\epsilon_1 \approx 10$, evaluated from our data) and the Josephson plasma suppressed down to 5 cm^{-1}.[12] These facts justify our assumption to set $\chi_{\rm int}$ equal to zero.

There are some distinct features in the spectra of Bi2212. The spectral weight of the anomalous phonon at 366 cm^{-1} is smaller than in Y123. Surprisingly, the ''bare'' oscillator strength of the phonon ($S_P = 1.09$) (Ref. 18) is quite similar to that for Y123 ($S_P = 1.3$),[16] which means that the phonon is strongly renormalized already in the normal state. This is caused by a large difference between the conductivity of intra- and inter-layers for Bi2212, which induces a strong charging effect within the bilayers and thus enhances the phonon renormalization due to the local field effect. Similar arguments can be used to explain the small spectral growth around 450 cm^{-1} in Bi2212, in contrast to a large bump in Y123.

The most dramatic changes in the spectra occur at T_c, indicating that the effects are related to the onset of superconductivity. A small gradual onset above T_c, which was observed for Y123,[1,2,19] has not been found. In the case of Y123, where the higher *c*-axis conductivity is due to the CuO chains in the inter-bilayers, the contribution of the free carriers was modeled by a very broad structureless term (strongly overdamped oscillator), which above T_c is reduced by pseudogap opening and below T_c by condensation.[16] The influence of the pseudogap effect is hardly seen in the *c*-axis spectra of Bi2212. This is related to the fact that the electronic background is very low already at room temperature. However, the low-ω suppression can be seen in the real and imaginary parts of the intra-bilayer conductivity obtained by fitting and shown in Fig. 4. It appears that the frequency dependence of the real part resembles the estimate[20] based on the ARPES data around the *X*-point in the Brillouin zone. Another interesting feature of the conductivity spectra is that, as the temperature is lowered, the mode at 366 cm^{-1} shifts very slightly to lower frequencies for the sample with $T_c = 80$ but in the opposite way for the $T_c = 60$ K sample. This is related to the fact that the frequency of the additional excitation is above the phonon frequency for the $T_c = 80$ K sample, whereas it is below it for the $T_c = 60$ K sample [similar doping dependence was found in Y123 (Ref. 16)].

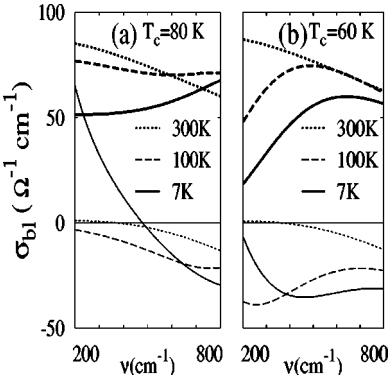

FIG. 4. Real (thick lines) and imaginary (thin lines) parts of the intrabilayer conductivity σ_{bl} for the $T_c = 80$ K sample (a) and the $T_c = 60$ K sample (b), obtained by fitting the data of Fig. 2.

In conclusion, we have studied the *c*-axis infrared response of underdoped Bi2212 ($T_c = 80$ K and 60 K). We found that the anomalies in the spectra (the additional band, the anomalous phonons) and their doping dependence are the same as in other bilayer cuprates. This shows that the anomalies are common features for the double pyramid materials, irrespective of the *c*-axis conductivity. The spectra can be very well described by the model including the intrabilayer plasmon and local field effects. This confirms that each CuO_2 plane should be regarded as an independent superconducting layer even within a double CuO pyramid. A small peak intensity for the oxygen bending phonon as well as a small intensity of the growing bump in Bi2212 can be understood as a consequence of enhanced local field effect due to the strong charging within a bilayer, which results from an insulating nature of the blocking layers. The present results demonstrate that the *c*-axis charge response cannot be treated as in a usual system, where electric field is homogeneous. In particular, the analysis of the spectral weight-changes in terms of the ''tight-binding'' sum rule[21,22] must be reconsidered, since this sum rule is derived assuming homogeneous

distribution of the total electric field, which is obviously not the case in HTSC.

This work has been supported by the New Energy and Industrial Technology Development Organization (NEDO) as Collaborative Research and Development of Fundamental Technologies for Superconductivity Applications and by Core Research for Evolutional Science and Technology Program of Japan Science and Technology Corporation. We would like to acknowledge D. van der Marel, C. Bernhard, and J. Humlíček for discussion and A. Yamamoto for the oxygen reduction of our samples.

*Permanent address: Institute of Physics, ASCR, Na Slovance 2, 182 21 Praha, Czech Republic.

[1] C. C. Homes, T. Timusk, R. Liang, D. A. Bonn, and W. N. Hardy, Phys. Rev. Lett. **71**, 1645 (1993).

[2] C. C. Homes *et al.*, Physica C **254**, 265 (1995); S. Tajima *et al.*, Phys. Rev. B **55**, 6051 (1997).

[3] K. Tamasaku, Y. Nakamura, and S. Uchida, Phys. Rev. Lett. **69**, 1455 (1992).

[4] D. N. Basov, T. Timusk, B. Dabrowski, and J. D. Jorgensen, Phys. Rev. B **50**, 3511 (1994).

[5] M. Reedyk, T. Timusk, J. S. Xue, and J. E. Greedan, Phys. Rev. B **49**, 15 984 (1994).

[6] A. P. Litvinchuk, C. Thomsen, and M. Cardona, Solid State Commun. **83**, 343 (1992).

[7] D. van der Marel and A. Tsvetkov, Czech. J. Phys. **46**, 3165 (1996).

[8] T. Motohashi *et al.*, Phys. Rev. B **59**, 14 080 (1999).

[9] S. Tajima, G. D. Gu, S. Miyamoto, A. Odagawa, and N. Koshizuka, Phys. Rev. B **48**, 16 164 (1993).

[10] W. E. Lawrence and S. Doniach, in *Proceedings of the 12th International Conference on Low Temperature Physics,* Kyoto, 1970, edited by E. Kanda (Keigaku, Tokyo, 1971), p. 361.

[11] R. Kleiner and P. Muller, Physica C **293**, 156 (1997).

[12] Y. Matsuda *et al.*, Phys. Rev. Lett. **75**, 4512 (1995); O. K. C. Tsui *et al.*, *ibid.* **76**, 819 (1996).

[13] M. Grüninger, D. van der Marel, A. A. Tsvetkov, and A. Erb, Phys. Rev. Lett. **84**, 1575 (2000).

[14] The appearance of the pole is a consequence of general properties of the dielectric function and boundary conditions. The excitation can be understood using an analogy to the optical phonons. It arises due to the presence of two different Josephson junctions in a unit cell.

[15] H. Shibata and T. Yamada, Phys. Rev. Lett. **81**, 3519 (1998).

[16] D. Munzar, C. Bernhard, A. Golnik, J. Humlíček, and M. Cardona, Solid State Commun. **112**, 365 (1999).

[17] J. Prade *et al.*, Phys. Rev. B **39**, 2771 (1989).

[18] The values of the parameters for the $T_c=80$ K sample: $\epsilon_\infty=4.05$, $\Omega_{bl}=2500$, $\gamma_{bl}=1180$, $\omega_1=327$, $\gamma_1=53$, $S_1=0.302$, $\omega_2=634$, $\gamma_2=54$, $S_2=0.464$, $\omega_P=449$, $\gamma_P=18$, $S_P=1.09$ at $T=300$ K; $\epsilon_\infty=4.05$, $\Omega_{bl}=2370$, $\gamma_{bl}=1180$, $\omega_b=861$, $\gamma_b=542$, $S_b=0.79$, $\omega_1=327$, $\gamma_1=53$, $S_1=0.302$, $\omega_2=637$, $\gamma_2=54$, $S_2=0.464$, $\omega_P=449$, $\gamma_P=20$, $S_P=1.09$ at $T=100$ K; $\epsilon_\infty=4.05$, $\omega_{bl}=969$, $\Omega_{bl}=1910$, $\gamma_{bl}=1180$, $\omega_b=1050$, $\gamma_b=975$, $S_b=2.33$ $\omega_1=327$, $\gamma_1=53$, $S_1=0.302$, $\omega_2=638$, $\gamma_2=61$, $S_2=0.464$, $\omega_P=449$, $\gamma_P=18$, $S_P=1.09$ at $T=7$ K. The values of the parameters for the $T_c=60$ K sample: $\epsilon_\infty=4.03$, $\Omega_{bl}=2570$, $\gamma_{bl}=1230$, $\omega_1=329$, $\gamma_1=53$, $S_1=0.279$, $\omega_2=636$, $\gamma_2=49$, $S_2=0.441$, $\omega_P=454$, $\gamma_P=18$, $S_P=1.03$ at $T=300$ K; $\epsilon_\infty=4.03$, $\Omega_{bl}=1290$, $\gamma_{bl}=1230$, $\omega_b=513$, $\gamma_b=1050$, $S_b=13.3$, $\omega_1=329$, $\gamma_1=53$, $S_1=0.279$, $\omega_2=639$, $\gamma_2=49$, $S_2=0.441$, $\omega_P=454$, $\gamma_P=24$, $S_P=1.03$ at $T=100$ K; $\epsilon_\infty=4.03$, $\omega_{bl}=623$, $\Omega_{bl}=437$, $\gamma_{bl}=1230$, $\omega_b=647$, $\gamma_b=1170$, $S_b=9.72$, $\omega_1=329$, $\gamma_1=53$, $S_1=0.279$, $\omega_2=639$, $\gamma_2=51$, $S_2=0.441$, $\omega_P=454$, $\gamma_P=58$, $S_P=1.03$ at $T=7$ K; The numerical factors used in our fitting procedure are $\alpha=2.28$, $\beta=0.64$, $\gamma=1.28$ (see Ref. 16 for definition).

[19] C. Bernhard *et al.*, Phys. Rev. B **61**, 618 (2000).

[20] C. Bernhard *et al.*, Phys. Rev. B **59**, R6631 (1999).

[21] S. Chakravarty, Hae-Young Kee, and E. Abrahams, Phys. Rev. Lett. **82**, 2366 (1999).

[22] D. N. Basov *et al.*, Science **283**, 49 (1999).